Materials and Design 191 (2020) 108660

Contents lists available at ScienceDirect

Materials and Design

journal homepage: www.elsevier.com/locate/matdes

Deformation behavior of annealed $Cu_{64}Zr_{36}$ metallic glass via molecular dynamics simulations

Xingxing Yue [a,*], Jamieson Brechtl [b], Fajie Wang [c], Zexin Chang [d], Peter K. Liaw [e], Cang Fan [a]

[a] School of Material Science and Engineer, Nanjing University of Science and Technology, Nanjing 210094, PR China
[b] The Bredesen Center for Interdisciplinary Research and Graduate Education, The University of Tennessee, Knoxville, TN 37996, USA
[c] School of Electromechanical Engineering, Qingdao University, Shandong 266071, PR China
[d] College of Materials Science and Engineering, Taiyuan University of Technology, Taiyuan 030024, PR China
[e] Department of Materials Science and Engineering, The University of Tennessee, Knoxville, TN 37996, USA

HIGHLIGHTS

- C14, C15 and five-fold local symmetry structures are observed in $Cu_{64}Zr_{36}$ metallic glass annealed isothermally at 950 K.
- Effect of temperature and strain rate on yield strength and stress drop of annealed $Cu_{64}Zr_{36}$ metallic glass is studied.
- Initial shear band results from the order-disorder transformation at 10 K and 5×10^7 s^{-1}.

GRAPHICAL ABSTRACT

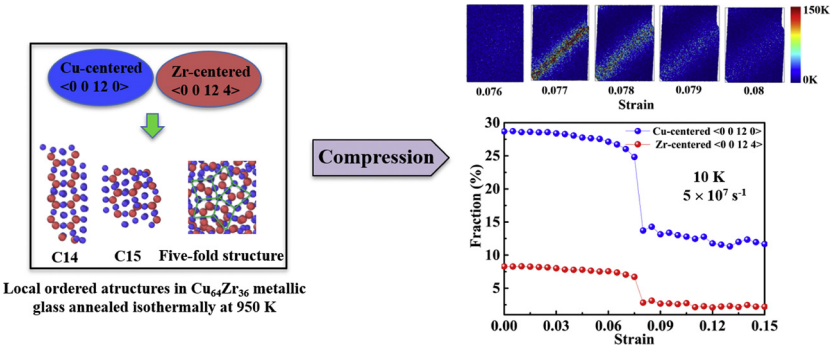

ARTICLE INFO

Article history:
Received 6 November 2019
Received in revised form 18 March 2020
Accepted 19 March 2020
Available online 20 March 2020

Keywords:
Molecular dynamics
$Cu_{64}Zr_{36}$ metallic glass
Annealing structure
Compression properties

ABSTRACT

In the present work, we investigate the isothermal annealing process of $Cu_{64}Zr_{36}$ metallic glass (MG) by means of molecular dynamics (MD) simulations, and characterize the compression properties under different temperatures and compressive rates. The pair distribution functions, the bond-orientational order, and the cluster-type index method are modeled and analyzed to characterize changes in the structure. Results of the modeling and analysis reveal that the $MgZn_2$-type Laves, $MgCu_2$-type Laves and five-fold local symmetry structures can be formed during the isothermal holding at 950 K. Study on the compression properties shows that at a fixed strain rate, the yield strength and yield drop all increase with decreasing temperature. At a fixed temperature, however, the increase of the strain rate leads to a noticeable increase in the yield strength at 600 K, but has little effect on yield strength at 10 K. Moreover, the modeling and analysis of the structure at a temperature of 10 K and strain-rate of 5×10^7 s^{-1} demonstrate that the order-disorder transformation initiates the shear band.

1. Introduction

Metallic glasses (MGs) are novel alloys with amorphous structures, which have many remarkable properties and therefore are promising for use in many fields [1–4]. However, there are still many issues and challenges that need to be addressed owing to the complex atomic structures of MGs [5]. There are three commonly used approaches for the study of MGs: experiments [6–9], theoretical [10–12] and computer simulations [13–17]. Among them, the computer simulations have become reliable and quite popular due to exponentially increasing computer power. The computer simulations cannot replace the

* Corresponding author.
E-mail address: yuexx90@163.com (X. Yue).

https://doi.org/10.1016/j.matdes.2020.108660

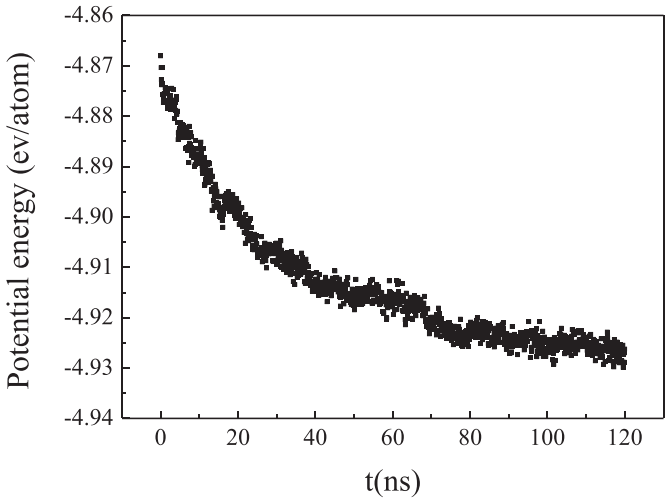

Fig. 1. The potential energy during the isothermal holding (for 950 K).

experiments completely, however, it can provide detailed knowledge and useful predictions at the atomic level. In numerous computer simulation studies of MGs, the Cu-Zr binary alloys have served as one of the research focuses [18–20], because it is not only one of the most popular bulk metallic glass-forming systems, but also easier to model and analysis than alloys with more elements.

Despite a lot of research efforts in the Cu-Zr metallic glasses, it still shows the great values of research and never failed to attract attention. The existing studies [21–23] on the Cu-Zr binary system always show that the icosahedral atomic structure plays an important role in the glass-forming ability (GFA), for example, the fraction of icosahedra in the matrix can be an indicator of GFA [22]. Recently, the nano-sized Cu_2Zr Laves phase was found in the $Cu_{64}Zr_{36}$ metallic glass via molecular dynamics (MD) simulations [24–26]. The Cu_2Zr Laves phase consists of the icosahedra and polyhedra with a coordination number of 16, demonstrating that the icosahedra in Cu-Zr system can also provide the possibility of crystallization.

By using MD simulations, the Cu_2Zr Laves phase has been confirmed in the annealed $Cu_{64}Zr_{36}$ metallic glass. However, the type of the crystal structure has not been identified, and some ordered structures could easily be ignored if one only observes a local section of annealed model. Moreover, it is also worth noting that a good understanding and knowledge of the mechanical properties is essential for the development of accurate and cost-effective design methods for metallic glasses, once the structure of the annealed $Cu_{64}Zr_{36}$ metallic glass is determined.

The purpose of this paper is to describe the microstructural evolution of the $Cu_{64}Zr_{36}$ metallic glass that was isothermally annealed above its glass transition temperature, to identify the type of crystal structure, and emphatically to investigate the compression behaviors of the annealed sample, by using MD simulations. In the study, the pair distribution functions (PDF), the bond-orientational order (BOO) and the cluster-type index method (CTIM), are employed to describe the details of the structure.

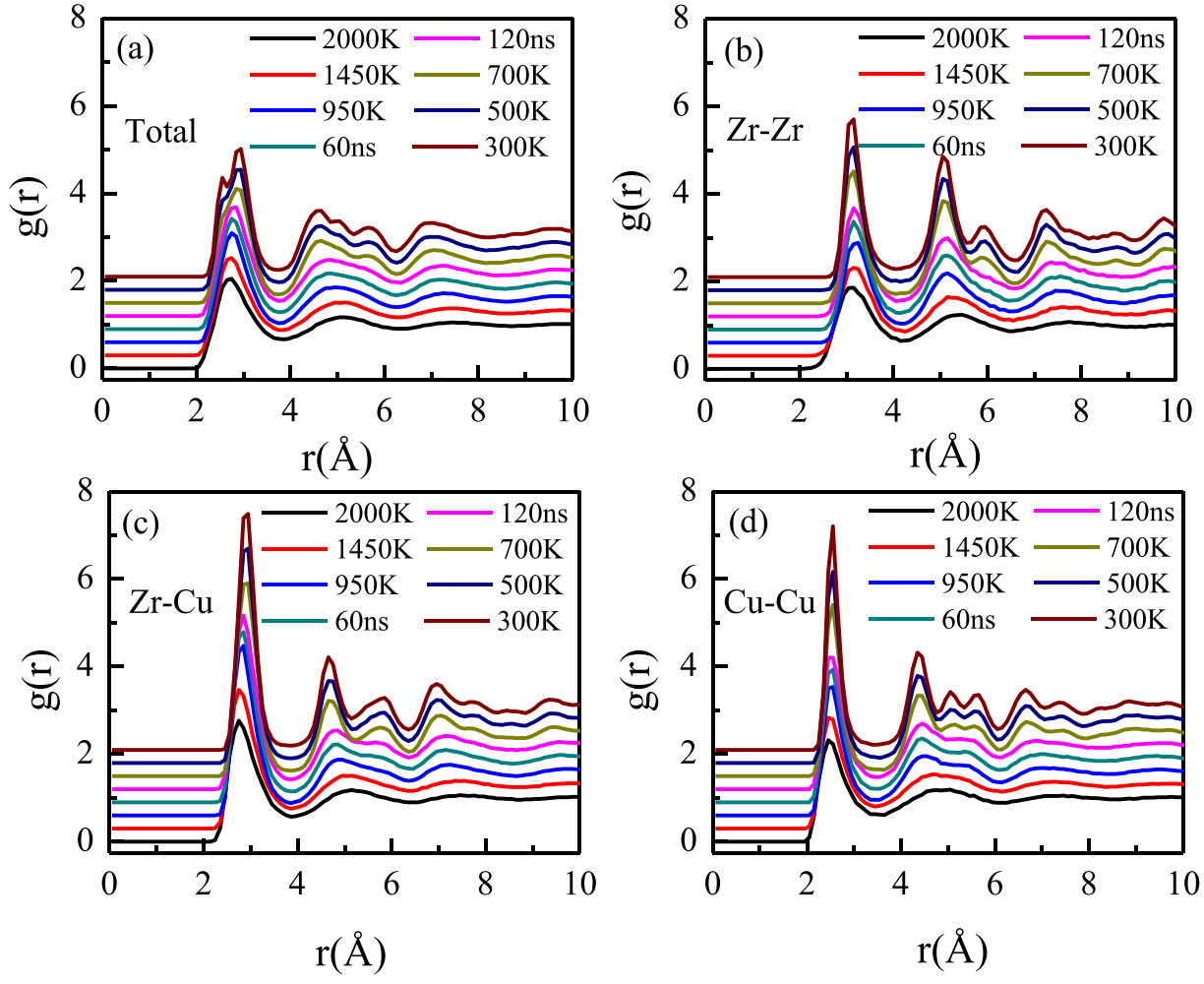

Fig. 2. The PDF curves during the isothermal holding and cooling process (300 K–2000 K) (a) total; (b) Zr-Zr; (c) Zr-Cu; and (d) Cu-Cu.

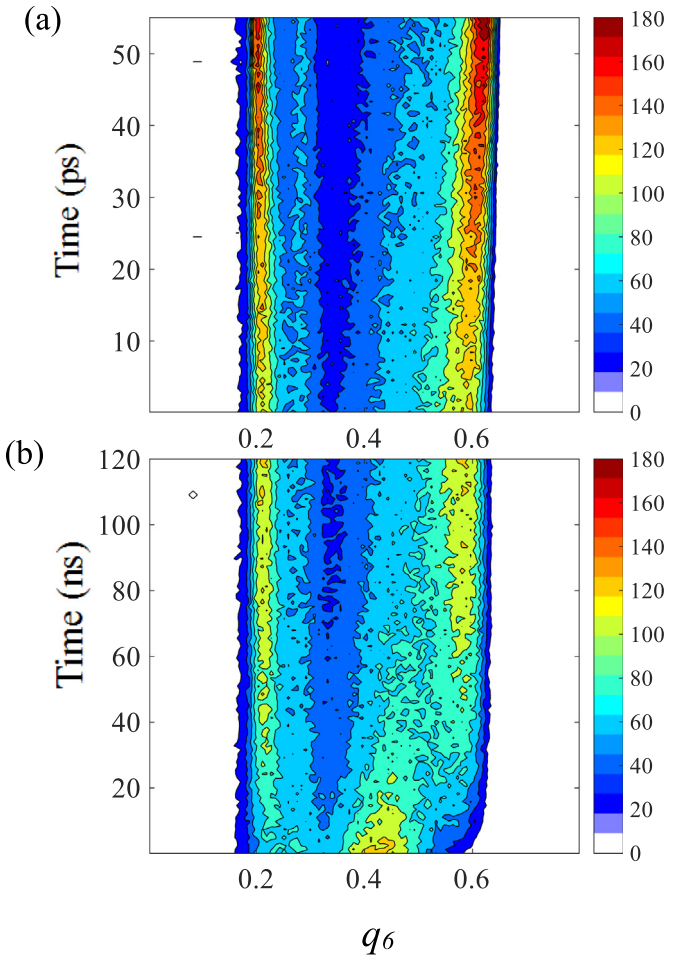

Fig. 3. Contours q_6 distribution in the annealing process: (a) cooling process after isothermal holding; and (b) isothermal holding. Colors represent the number of atoms with specific q_6 values.

The rest of this paper is organized as follows. Section 2 provides the detailed information of MD simulations for the isothermal annealing process and compression tests. Section 3 illustrates the structure evolution of the $Cu_{64}Zr_{36}$ metallic glass during isothermal annealing, and presents the stress-strain curves of annealed sample using compression tests at different strain rates and temperatures. In Section 4, the structural change during deformation is discussed. Finally, some concluding remarks are given in Section 5.

2. Methods

The MD simulations were performed, using the large-scale atomic/molecular massively-parallel simulator (LAMMPS) program package [27]. The Cheng's embedded type atomic interactions were used to describe the interaction between atoms [28]. A time step of 1 fs was used, and the periodic boundary condition was applied in the x, y, and z directions. In our previous work, the glass-transition temperature for the $Cu_{64}Zr_{36}$ metallic glass is ~770 K when the liquid is rapidly cooled, using a cooling rate of 10^{12} K/s via the MD simulations [29]. To obtain the annealed sample, a number of steps were performed. Firstly, a simulation system containing 4320 Cu and 2430 Zr atoms was equilibrated at 2000 K to obtain the liquid structure. Secondly, the liquid structure was cooled to 950 K using a cooling rate of 10^{12} K/s and isothermal holding for 120 ns. Finally, the structure was cooled to 300 K using the beforementioned cooling rate and then relaxed for 1 ns.

To simulate compressive deformation, a simulation model containing 162,000 atoms was initially built from $4 \times 6 \times 1$ replicas (in x, y, and z direction). The replicas were based on the structure of the annealed $Cu_{64}Zr_{36}$ metallic glass configuration (obtained above). The system was subsequently relaxed at 950 K for 0.5 ns, and then the temperature was reduced to three different temperatures using a cooling rate of 10^{12} K/s. The final temperatures were 10 K, 300 K, and 600 K. The mechanical behavior was simulated via uniaxial compression along the y axis using constant deformation rates (5×10^7 s^{-1}, 10^8 s^{-1}, and 5×10^8 s^{-1}) and different temperatures (10 K, 300 K, and 600 K). The x direction was set as the free surface to enable the shear offset on this surface. The y and z directions were set as periodic boundaries. From the simulations, the stress-strain curves were obtained for the different experimental conditions. Noting that all the stress-strain curves are tested only once. Because the simulation overcomes the man-made errors and environment influence.

Table 1
The number of the most abundant 8 clusters.

Cluster type	Number
Cu (12 12/1551)	2093
Cu (12 8/1551 2/1541 2/1431)	363
Cu (12 8/1551 2/1441 2/1661)	140
Cu (11 6/1551 2/1541 2/1431 1/1441)	113
Zr (16 12/1551 4/1661)	642
Zr (16 9/1551 3/1541 1/1431 3/1661)	144
Zr (15 9/1551 3/1541 1/1431 2/1661)	130
Zr (15 12/1551 3/1661)	113

3. Results

Fig. 1 presents the potential energy of the system as a function of the annealing time for a temperature of 950 K. The potential energy decreases monotonically as the annealing time increases, and the reduction rate is noticeably higher for $t < 40$ ns. The decrease in the potential energy is attributed to the rearrangement of the amorphous atoms into a more ordered state.

The PDF, $g(r)$, is a structural parameter that is typically used to determine the primary structural characteristics of the liquid, amorphous, and crystalline states [30]. It is a pair correlation representing the probability of finding atoms at a distance, r, away form a reference atom. The total PDF is expressed as follows:

$$g(r) = \frac{V}{N^2}\left\langle \sum_{i=1}^{N} \frac{n_i(r)}{4\pi r^2 \Delta r} \right\rangle, \tag{1}$$

where V is the volume of simulation system, N is the total number of atoms, and $n_i(r)$ is the number of atoms around the ith atom within the radius, r to $r + \Delta r$ of spherical shells. For the partial PDF, the format is written as

$$g_{\alpha\beta} = \frac{V}{N_\alpha N_\beta}\left\langle \sum_{i=1}^{N_\alpha} \frac{n_{i\beta}(r)}{4\pi r^2 \Delta r} \right\rangle, \tag{2}$$

where N_α and N_β are the numbers of type α and β atoms, respectively.

To help elucidate the microstructural evolution during the entire simulation process, the PDF curves for eight temperatures are depicted in Fig. 2(a)–(d). Here, Fig. 2(a) displays the total PDF, $g_{total}(r)$, while Fig. 2(b) presents the partial PDF function, $g_{Zr\text{-}Zr}(r)$, for the Zr atoms. Additionally, Fig. 2(c) shows the partial PDF, $g_{Zr\text{-}Cu}(r)$, for the Zr and Cu atoms, and Fig. 2(d) represents the partial PDF, $g_{Cu\text{-}Cu}(r)$, for the Cu atoms. For a temperature of 2000 K, the PDF curves exhibit a pattern that is characteristic of an amorphous (liquid) structure. As the temperature decreases, the second peak of $g_{Zr\text{-}Zr}(r)$ [Fig. 2(b)] becomes narrower and more pronounced, whilst the second peak of $g_{Zr\text{-}Cu}(r)$ [Fig. 2(c)] and $g_{Cu\text{-}Cu}(r)$ [Fig. 2(d)] decomposes into two peaks, signifying an enhancement of the atomic ordering. During the isothermal

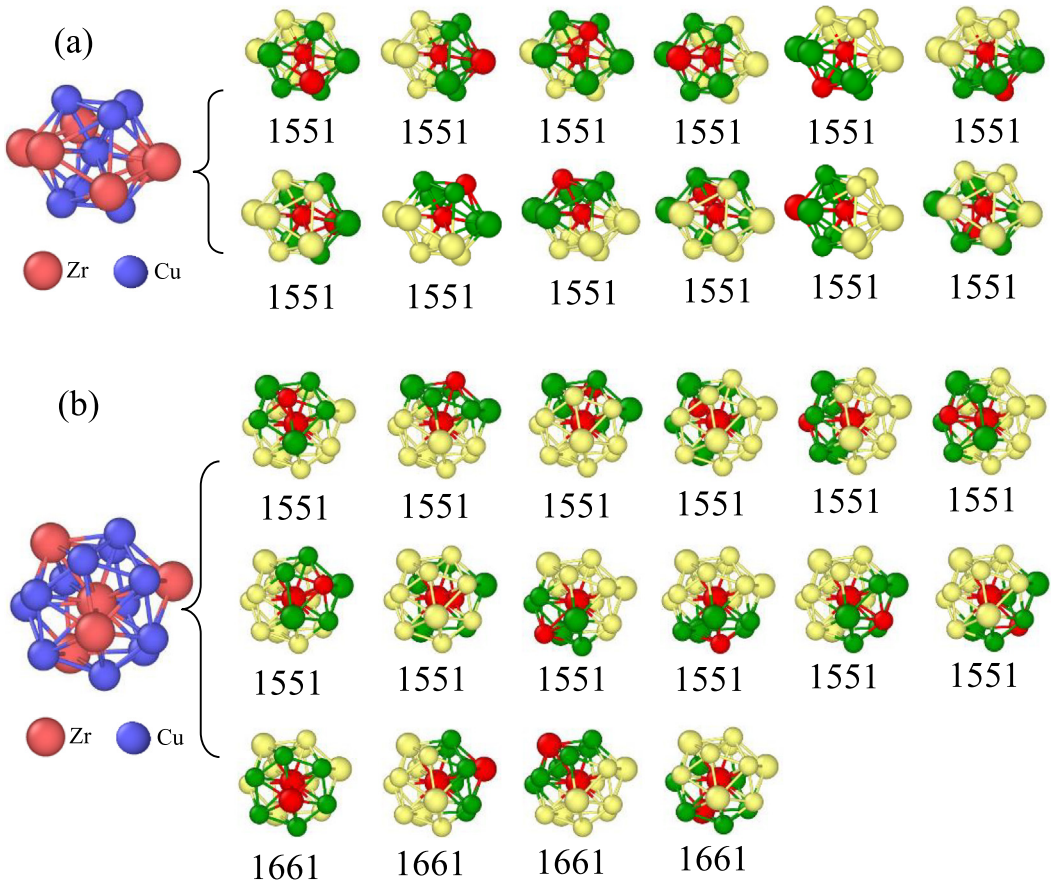

Fig. 4. Schematic diagram of the (a) Cu-centered (12 12/1551) cluster; and the (b) Zr-centered (16 12/1551 4/1661) cluster. The red balls are the root pair atoms, the green balls are the near-neighbor atoms shared in common around root pair, the yellow balls are the rest atoms in the cluster.

holding at 950 K, the second peak of $g_{Zr\text{-}Cu}(r)$ [Fig. 2(c)] and $g_{Cu\text{-}Cu}(r)$ [Fig. 2(d)] exhibits a more pronounced peak splitting with an increase in the annealing time. During the subsequent cooling process, there is a noticeable change in these PDF curves, where the second peak of $g_{Zr\text{-}Zr}(r)$ [Fig. 2(b)] splits into two peaks. The subpeak of the second peak of $g_{Cu\text{-}Cu}(r)$ [Fig. 2(d)] decomposes into two smaller peaks. Furthermore, the third peak ($r > 6$ Å) in Fig. 2(b)–(d) of these curves also exhibits significant changes. For instance, the third peak splits into two peaks in which their magnitude increases with a decrease in the temperature. It may be surmised from Figs. 2(a)–(d) and 1 that the crystal nucleation occurs when the system is subjected to isothermal holding at 950 K. After the isothermal holding, rapid quenching is applied to the system, where the rapid growth of the crystal nuclei occurs.

To further study the structural information of the isothermal holding and subsequent quenching process, the BOO parameter [31] is analyzed from the MD simulation results to evaluate the local structural ordering. The BOO parameter is defined as

$$q_l(i) = \left(\frac{4\pi}{2l+1} \sum_{m=-l}^{l} |q_{lm}(i)|^2 \right)^{1/2}, \tag{3}$$

Here,

$$q_{lm}(i) = \frac{1}{N_b(i)} \sum_{j=1}^{N_b} (i) Y_{lm}(\mathrm{r}_{ij}), \tag{4}$$

where $N_{b(i)}$ is the number of the nearest neighbors of atom, i, Y_{lm} is the spherical harmonic function with degree, l is the free integer parameter, and m is an integer that changes from - l to l. Among the q_l parameters, q_6 is sensitive to measure the local structure features.

Fig. 3(b) and (a) present the contours of the q_6 distribution that results from the isothermal holding and the subsequent quenching process, respectively. Colors denote the number of atoms with specific q_6 values. For $t <$ ~20 ns, the atoms are most concentrated for the q_6 values ranging from 0.37 to 0.48 [see Fig. 3(b)]. With an increase in the annealing time, the maximum q_6 value increases to ~0.62. In the following quenching process [see Fig. 3(a)], the number of atoms is most concentrated for the q_6 values centered around 0.2 and 0.6. For the high concentration of atoms that are centered around the latter value ($q_6 =$ 0.6), the number of atoms in this region increases at a faster rate, as compared to the isothermal holding process. Moreover, it can be observed in Fig. 3(a) that for the cooling process, the maximum q_6 value of the profile is shifted to the right ($q_6 > 0.6$). It has been reported that the q_6 values for icosahedral symmetry structure is 0.663 [32] and the atoms with the q_6 values of ~0.2 correspond to a coordination number of 16 [26]. Based on the above results, therefore, the annealing process leads to the generation of crystal structures that consist of icosahedra and clusters with a coordination number of 16.

To obtain the detailed structural information of the annealed sample (300 K), its microstructure was analyzed, using the cluster-type index method (CTIM) [33]. For this method, the local structure is defined as [Z, n/(ijkl), …], where Z is the coordination number around the central atoms, and n/(ijkl) is the number of (ijkl) H-A bond-types. Table 1 presents the 8 most abundant clusters whose numbers are >100. For the Cu-centered clusters, the icosahedron (12 12/1551) is the most abundant type, followed by the distorted icosahedron Cu (12 8/1551 2/1541 2/1431) and Cu (12 8/1551 2/1441 2/1661). For the Zr-centered clusters, it can be observed that (16 12/1551 4/1661) is more abundant than the other Zr-centered clusters. Fig. 4 shows the schematic diagram of these two populous clusters characterized by the CTIM. According to

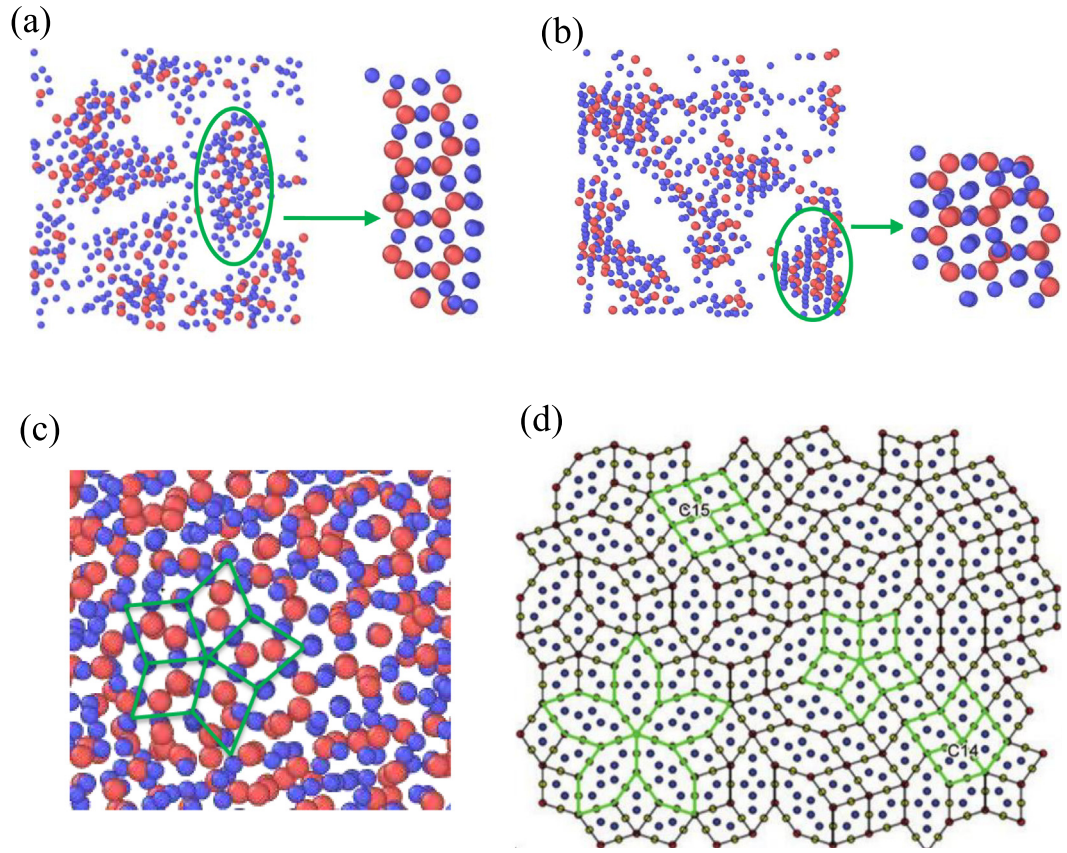

Fig. 5. (a) local structure of the $MgZn_2$-type laves structure; (b) local structure of the $MgCu_2$-type laves structure; (c) five-fold symmetry structure; (d) modeled atomic arrangement of the precipitate-rod in Mg-Zn alloy [34].

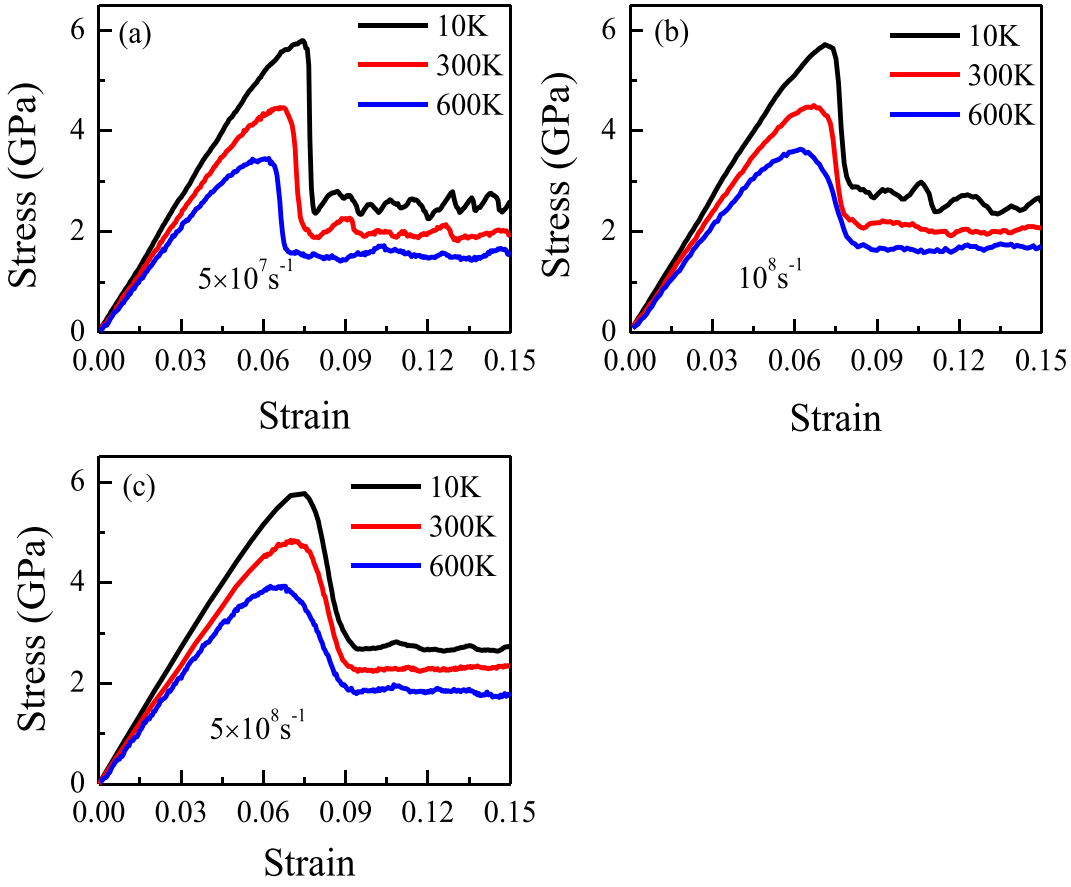

Fig. 6. Stress-strain curves for temperatures of 10 K, 300 K, and 600 K at a strain rate of (a) $5 \times 10^7\ s^{-1}$, (b) $10^8\ s^{-1}$, and (c) $5 \times 10^8\ s^{-1}$.

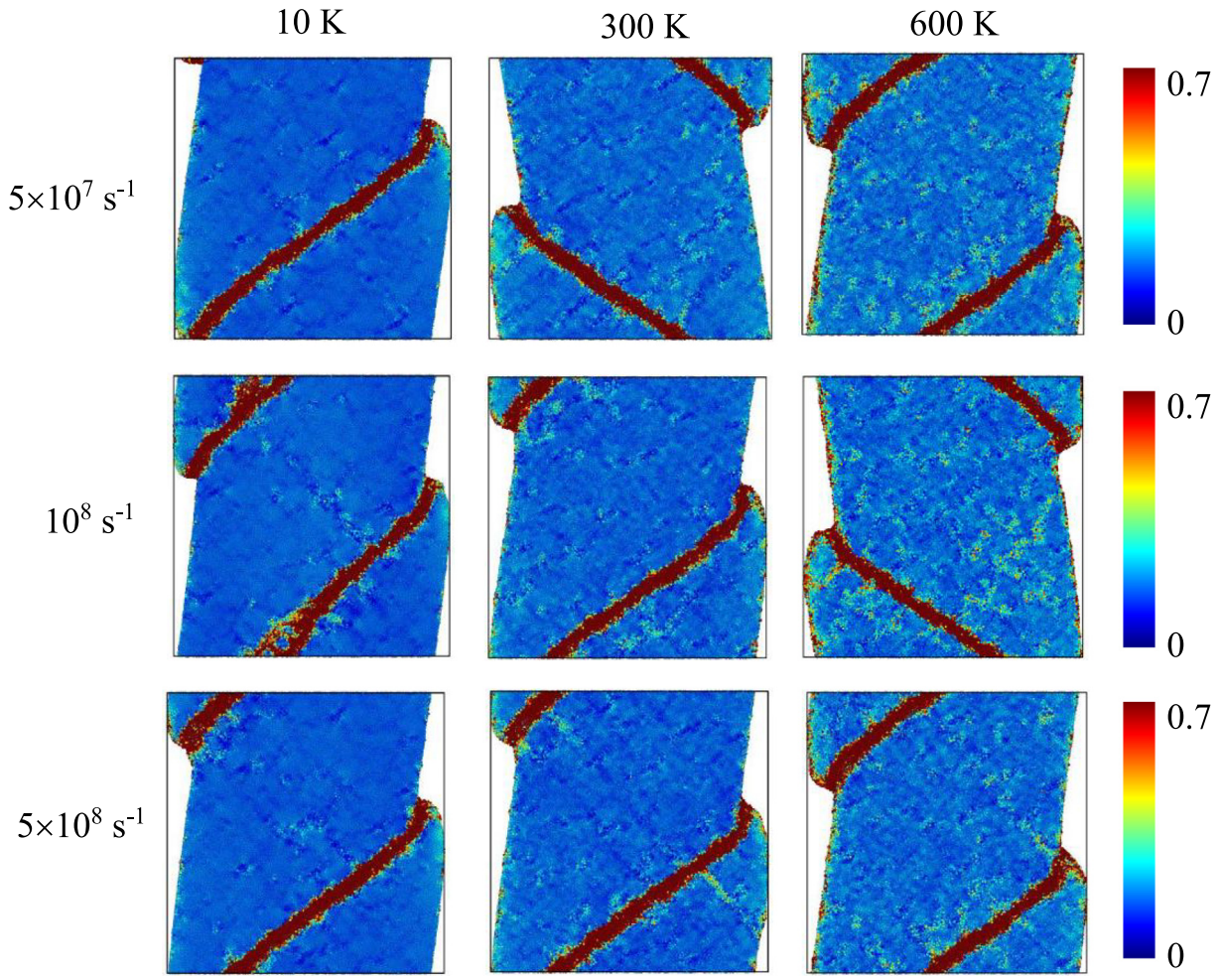

Fig. 7. Snapshots of samples at a strain of 15%. The samples are deformed in compression test under temperatures of 10, 300, and 600 K, and strain rates of 5×10^7 s^{-1}, 10^8 s^{-1}, and 5×10^8 s^{-1}.

the BOO analysis, it can be concluded that the Cu-centered (12 12/1551) and Zr-centered (16 12/1551 4/1661) are the products of crystallization, which can also be characterized by a Voronoi polyhedra of type Cu-centered <0 0 12 0> and Zr-centered <0 0 12 4>. Observing the snapshot of the central atoms of these two clusters in 1-nm thick layer of simulation system, it can be found that the nano-size domains in Fig. 5(a) and (b) are the local structure of the $MgZn_2$-type (C14) and $MgCu_2$-type (C15) Laves structure, respectively. Moreover, we also see a five-fold symmetry structure in a layer. In order to identify this structure clearly, Fig. 5(c) presents a part of this layer with all the atoms. It is worth noting that recently, Qin et al. [34] found a new class of intermediate structure containing the short-range ordered C14 and C15 and two kinds of 2D five-fold symmetry locally, as shown in Fig. 5(d). We can find that five-fold structure in Fig. 5(c) is similar to the one of five-fold

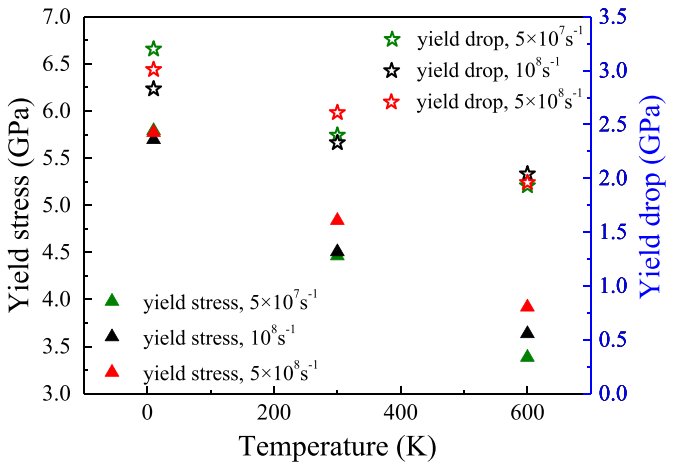

Fig. 8. The change of yield strength and yield drop with the temperature and strain rate.

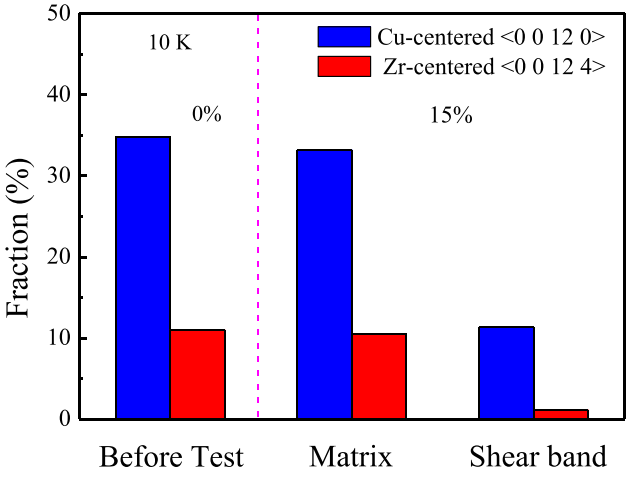

Fig. 9. Comparison of the Cu_2Zr Laves phase at strains of 0% and 15%.

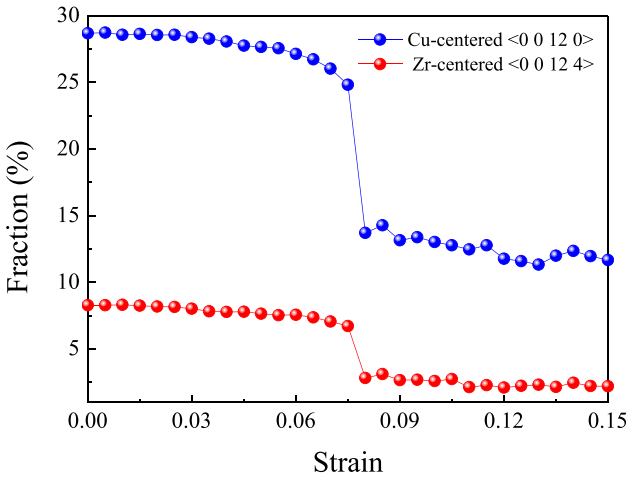

Fig. 10. The fractions of Cu-centered <0 0 12 0> and Zr-centered <0 0 12 4> polyhedron as a function of strain in the region that evolves into the shear band.

nanodomain structures in Fig. 5(d). Therefore, there are three kinds of ordered structure in the annealed system, maybe these ordered structures during annealing compete with each other and finally relax into stable crystal, or maybe this annealing process tend to form the structure which similar with Qin's finding.

For the annealed system, it is vitally important to know the corresponding mechanical properties. Fig. 6 shows the temperature dependence of the compressive stress-strain curves observed for strain rates ranging from 5×10^7 s^{-1} to 5×10^8 s^{-1}. The characteristics of these stress-strain curves are very similar. In the elastic-deformation region, the stress-strain curves show the linear behavior. After the yielding point is reached, the plastic deformation begins, and shortly thereafter, the compressive stress reaches the peak strength. Subsequently, a sudden, rapid drop in the stress occurs, which indicates that the deformation is localized into shear bands, as can be seen in Fig. 7. After yielding, the plastic flow stress fluctuates about a constant value. Interestingly, at the temperature of 10 K and strain rate of 5×10^7 s^{-1}, the stress-strain curve shows the obvious serrated flow phenomena.

Fig. 8 shows the yield strength and yield drop values for temperatures and strain rates ranging from 10 K– 600 K and 5×10^7 s^{-1}–5×10^8 s^{-1}, respectively. With decreasing the temperature from 600 to 10 K, the yield strength increases, indicating the strong temperature dependence of yield strength. The concentration of the free-volume zone can lead to a concentration of the local shear stress [35]. At 10 K, the thermodynamic mobility of atoms decreases and the bonds between the atoms become stiffer, leading to a difficulty of free-volume accumulation and creation. Therefore, the higher applied stress for the nucleation of the shear band is needed at 10 K, resulting in an increase in the yield strength. In addition, it can be observed that the yield strength increases with the increase of strain rate at 600 K. However, at 10 K, the strain rate has little effect on the yield strength. Therefore, it can be concluded that the strain rate sensitivity of yield strength decreases as the decreasing the temperature. For the yield drop, it can be seen that the yield drop increases with decreasing temperature for a given strain rate. However, at a constant temperature the yield drop shows no definite trend with respect to a change in the strain rate.

4. Discussion

The above results clearly show that the stress-strain curve of the annealed $Cu_{64}Zr_{36}$ metallic glass exhibits a large yield drop and obvious serrated flow at 10 K and 5×10^7 s^{-1}. Therefore, we explore the structural change during this deformation, and study the structure-mechanical properties relationships.

The result of structural analysis has shown that there are three kinds of ordered structure in the annealed $Cu_{64}Zr_{36}$ metallic glass, all of these ordered structures consist of Cu-centered <0 0 12 0> and Zr-centered <0 0 12 4> clusters. Here, the contents of these two kinds of clusters were calculated at strains 0% and 15%, as presented in Fig. 9. After deformation, the fraction of these two kinds of clusters in the matrix was quite similar to that of the sample that was subjected to virtually no strain. However, the fraction of these clusters in the shear band was significantly lower than that in the matrix. This demonstrates that most structural changes occur within shear band.

To gain a better understanding of how the fraction of polyhedron changes in the shear band during deformation, the fraction of some popular polyhedra as a function of strain in the region that evolves into the shear band, was analyzed. The results are presented in Fig. 10, and as can be seen, the sudden reduction (at 7.5%–8% strain) of the Cu-centered <0 0 12 0> and Zr-centered <0 0 12 4> clusters indicates that the mixed ordered structure was annihilated in the shear band during deformation. This result is consistent with that reported in Ref. [36].

The annihilation of the ordered structure must be accompanied by a change in structural characteristics. In order to investigate this issue, we calculate the number of the polyhedral type that are converted from the Cu-centered <0 0 12 0> and Zr-centered <0 0 12 4> polyhedra, as a function of the strain. As shown in Fig. 11(a)–(b), in general, the number of the polyhedral type increases with increasing strain, then evidently shows a sudden increase of 7.5% - 8% in the strain, and then varies over a small range. The increase of the polyhedral type tentatively

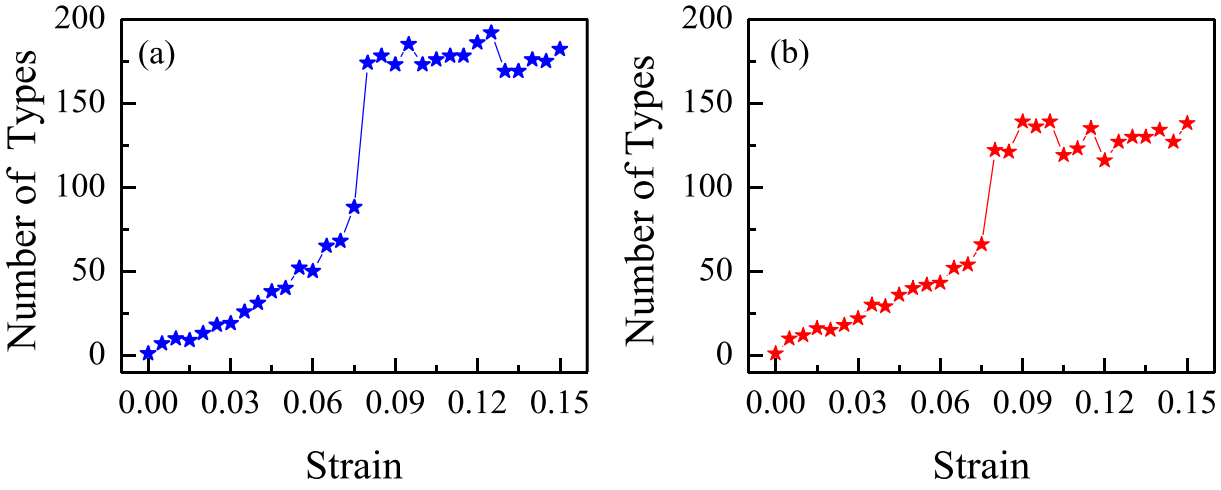

Fig. 11. The number of polyhedral type transformed from (a) Cu-centered <0 0 12 0> polyhedra and (b) Zr-centered <0 0 12 4> polyhedra.

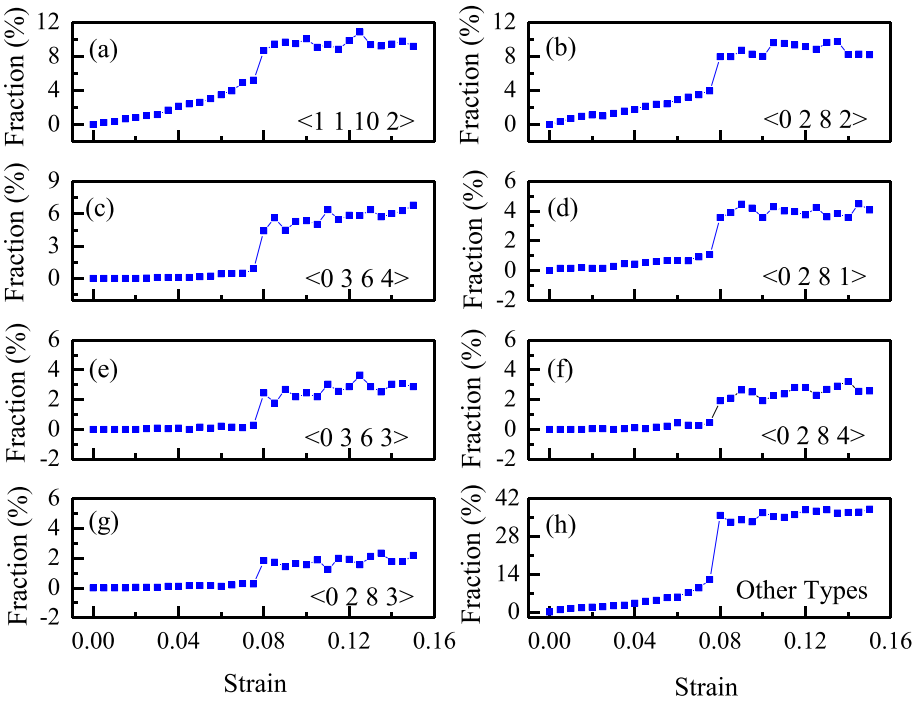

Fig. 12. The evolution of Cu-centered <0 0 12 0> polyhedra during deformation.

indicates that the ordered structure in the shear band turns into a disordered state.

To further evaluate the variation of the specific polyhedral type in Fig. 11, the fractions of 7 popular and the other types of polyhedra as a function of the applied strain are evaluated. These results are displayed in Figs. 12 and 13. In Fig. 12, when the strain is below 0.075, the icosahedra that evolve into the shear band transforms into the <0 1 10 2>, <0 2 8 2>, and <0 2 8 1> polyhedra. The fractions of these polyhedra change within 5%. When the strain reaches a value of 0.08, the fraction of the <0 1 10 2>, <0 2 8 2>, and <0 2 8 1> suddenly increase from values of 5.5%, 3.9%, and 1.1% to 9.54%, 8.8%, and 4.0%, respectively. Moreover, the fraction of the <0 3 6 4>, <0 3 6 3>, <0 2 8 4>, and <0 2 8 3> polyhedra increase from 0% to 5.7%, 2.7%, 2.5% and 1.8%, respectively. However, as shown in Fig. 12(h), most of the icosahedra transform into other types of polyhedra, where the fraction of the other types polyhedra increases from 12.1% to 36.1% when the strain exceeds 0.075. For the Zr-centered <0 0 12 4> polyhedra, as shown in Fig. 13, most of them also transform into other types of polyhedra. Therefore, we can definitely conclude that the order-disorder transformation occurs in the shear band. That is to say, the ordered structure in the shear band is annihilated and turns

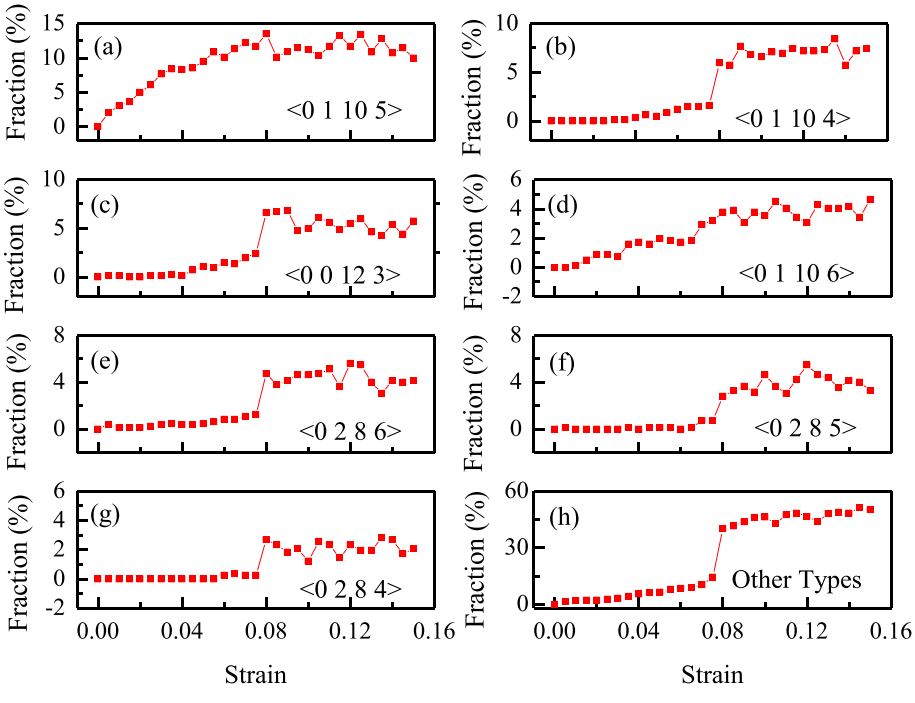

Fig. 13. The evolution of Zr-centered <0 0 12 4> polyhedra during deformation.

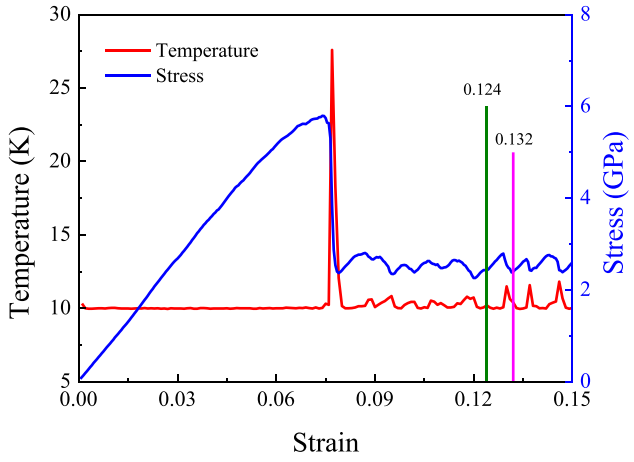

Fig. 14. The variation of temperature and stress during compression. The stress-strain curve between the green and pink is one of the serrations.

into a disordered structure. In addition, it is worth noting that the initial stress drop in stress-strain curve is also at ~7.5%–8% strain, illustrating that the abrupt decrease of the stress is accompanied by the order-disorder transformation.

Under uniaxial compression, the stored elastic-strain energy during the elastic-loading process can be converted into heat, which would affect the mechanical behavior significantly [37,38]. Fig. 14 presents the variation of temperature and stress during compression. The temperature is calculated using $T = 2E_k/3k_b$ (E_k is the average kinetic energy of atoms, K_b is the Boltzmann constant). It can be clearly found that the abrupt rise in temperature apparently follows the initiation of the stress-drop event. This indicates that the order-disorder transformation results in the initial shear band rather than the thermal activities.

In Fig. 14, the abrupt drop in stress corresponds to a rapid increase and decrease of the temperature when the strain changes from 7.6% to 8%. Then in the subsequent serrated flow, the correlation between the stress and temperature remains similar characteristics. For example, for strains that range from 12.4% to 13.2%, the stress drop of the serration is accompanied by a similar increasing and decreasing trend in the temperature. This demonstrates that the serrated flow has a relationship with thermal activity. In addition, it is evident that the temperature decreases to almost zero during the stress drop. In order to visualize the temperature distribution, we calculate the temperature of the sample at strain of 7.6% to 8%, as presented in Fig. 15. It can be seen that the rise in the temperature (141 K) of the shear band is followed by a dramatic decrease in the local temperature. This decrease in the temperature corresponds to a dissipation of the thermal energy into the surrounding matrix. Therefore, it can be inferred that the thermal activity is difficult to cause the fracture due to the insufficient heat.

5. Conclusions

Using the MD simulations, we have studied the structural evolution of the $Cu_{64}Zr_{36}$ metallic glass that was isothermally annealed above the glass transition temperature (950 K), and then analyzed the compression properties of annealed samples that were subjected to temperatures of 10 K, 300 K and 600 K, and strain rates ranging from 5×10^7 s^{-1} to 5×10^8 s^{-1}. It was found that the $Cu_{64}Zr_{36}$ metallic glass partially crystallizes during annealing at 950 K. Specifically, the crystallized structure is mixed with $MgZn_2$-type Laves, $MgCu_2$-type Laves, and five-fold local symmetry structures. As for the compression properties, it is greatly affected by the temperature and strain rate. Importantly, the serrations are visible in the stress-strain curve, especially at a temperature of 10 K and strain-rate of 5×10^7 s^{-1}. During this compression test, the order-disorder transformation causes the initial shear band. Moreover, the temperature fluctuations in the shear band preliminarily demonstrates that the thermal activity is associated with serration behavior, but is difficult to cause the fracture because of the insufficient heat.

It is worth noting that in our MD simulations, the type of serration is not regular, and the sample does not fracture at 15% strain. Therefore, a more detailed and rigorous effect of the thermal activities on the serration behavior and fracture needs to be illuminated, as well as the studies on the fractured surfaces. Future work will focus on investigating these problems.

CRediT authorship contribution statement

Xingxing Yue: Conceptualization, Investigation, Writing - original draft. **Jamieson Brechtl:** Resources, Writing - review & editing. **Fajie Wang:** Software, Resources. **Zexin Chang:** Software. **Peter K. Liaw:** Supervision, Writing - review & editing. **Cang Fan:** Resources, Supervision.

Declaration of competing interest

The authors declare that they have no known competing financial interests or personal relationships that could have appeared to influence the work reported in this paper.

Acknowledgments

The present work was supported by the NSFC (Grant No. 50971057 and 51371099). PKL is very grateful for the financial support of the National Science Foundation (DMR-1611180 and 1809640) with Drs. G. Shiflet and D. Farkas as program managers.

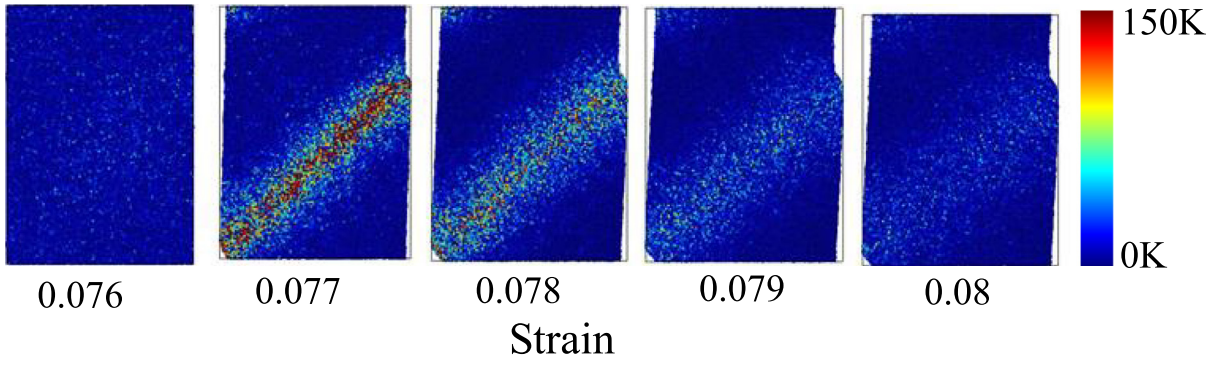

Fig. 15. Distribution of the temperature in the sample from 7.6% to 8% strains. The local temperature is calculated by averaging the kinetic energy of a group of atoms and then denotes it in Kelvin.

References

[1] L. Liu, C.L. Qiu, C.Y. Huang, Y. Yu, H. Huang, S.M. Zhang, Biocompatibility of Ni-free Zr-based bulk metallic glasses, Intermetallics 17 (2009) 235–240.
[2] B. Nair, G. Priyadarshini, Process, structure, property and applications of metallic glasses, AIMS Mater. Sci. 3 (2016) 1022–1053.
[3] P. Wang, J.Q. Wang, H. Li, H. Yang, J. Huo, J. Wang, C. Chang, X. Wang, R.W. Li, G. Wang, Fast decolorization of azo dyes in both alkaline and acidic solutions by Al-based metallic glasses, J. Alloy. Compd. 701 (2017) 759–767.
[4] M.M. Khan, A. Nemati, Z.U. Rahman, U.H. Shah, H. Asgar, W. Haider, Recent advancements in bulk metallic glasses and their applications: a review, Crit. Rev. Solid. State. 43 (2018) 233–268.
[5] W.H. Wang, Dynamic relaxations and relaxation-property relationships in metallic glasses, Prog. Mater. Sci. (2019), 100561.
[6] D.C. Hofmann, G. Duan, W.L. Johnson, TEM study of structural evolution in a copper mold cast $Cu_{46}Zr_{54}$ bulk metallic glass, Scripta. Mater. 54 (2006) 1117–1122.
[7] J. Pan, Q. Chen, N. Li, L. Liu, Formation of centimeter Fe-based bulk metallic glasses in low vacuum environment, J. Alloy. Compd. 463 (2008) 246–249.
[8] J. Saida, R. Yamada, M. Wakeda, S. Ogata, Thermal rejuvenation in metallic glasses, Sci. Technol. Adv. Mat. 18 (2017) 152–162.
[9] L. Deng, A. Gebert, L. Zhang, H.Y. Chen, D.D. Gu, U. Kühn, M. Zimmermann, K. Kosiba, S. Pauly, Mechanical performance and corrosion behaviour of Zr-based bulk metallic glass produced by selective laser melting, Mater. Design. 189 (2020) 108532.
[10] P. Thamburaja, Length scale effects on the shear localization process in metallic glasses: a theoretical and computational study, J. Mech. Phys. Solids. 59 (2011) 1552–1575.
[11] T.C. Hufnagel, C.A. Schuh, M.L. Falk, Deformation of metallic glasses: recent developments in theory, simulations, and experiments, Acta Mater. 109 (2016) 375–393.
[12] X. Yue, A. Inoue, C.T. Liu, C. Fan, The development of structure model in metallic glasses, Mater. Res-Ibero-Am. J. 20 (2017) 326–338.
[13] M. Zink, K. Samwer, W.L. Johnson, S.G. Mayr, Plastic deformation of metallic glasses: size of shear transformation zones from molecular dynamics simulations, Phys. Rev. B 73 (2006), 172203.
[14] M. Widom, B. Sauerwine, A.M. Cheung, S.J. Poon, P. Tong, D. Louca, G.J. Shiflet, Elastic properties of Ca-based metallic glasses predicted by first-principles simulations, Phys. Rev. B 84 (2011), 054206.
[15] H. Tian, C. Zhang, L. Wang, J. Zhao, C. Dong, B. Wen, Q. Wang, Ab initio molecular dynamics simulation of binary $Cu_{64}Zr_{36}$ bulk metallic glass: validation of the cluster-plus-glue-atom model, J. Appl. Phys. 109 (2011), 123520.
[16] A. Mahata, M.A. Zaeem, M.I. Baskes, Understanding homogeneous nucleation in solidification of aluminum by molecular dynamics simulations, Model. Simul. Mater. Sc. 26 (2018), 025007.
[17] S.D. Feng, K.C. Chan, L. Zhao, S.P. Pan, L. Qi, L.M. Wang, R.P. Liu, Rejuvenation by weakening the medium range order in $Zr_{46}Cu_{46}Al_8$ metallic glass with pressure preloading: a molecular dynamics simulation study, Mater. Design. 158 (2018) 248–255.
[18] C.C. Wang, C.H. Wong, Structural properties of $Zr_xCu_{90-x}Al_{10}$ metallic glasses investigated by molecular dynamics simulations, J. Alloy. Compd. 510 (2012) 107–113.
[19] X.F. Zhang, S.P. Pan, J.W. Qiao, A.D. Lan, Effect of Al on the atomic structure in $Zr_{50}Cu_{40}Al_{10}$ metallic glass, Comput. Mater. Sci. 128 (2017) 343–347.
[20] C.X. Peng, D. Şopu, Y. Cheng, K.K. Song, S.H. Wang, J. Eckert, L. Wang, Deformation behavior of designed dual-phase CuZr metallic glasses, Mater. Design. 168 (2019), 107662.
[21] Z.D. Sha, Y.P. Feng, Y. Li, The fundamental structural factor in determining the glass-forming ability and mechanical behavior in the Cu-Zr metallic glasses, Mater. Chem. Phys. 127 (2011) 292–295.
[22] B.F. Lu, J.F. Li, L.T. Kong, Y.H. Zhou, Correlation between mechanical behavior and glass forming ability of Zr-Cu metallic glasses, Intermetallics 19 (2011) 1032–1035.
[23] Z.C. Xie, T.H. Gao, X.T. Guo, X.M. Qin, Q. Xie, Growth of icosahedral medium-range order in liquid TiAl alloy during rapid solidification, J. Non-Cryst. Solids 394 (2014) 16–21.
[24] J. Zemp, M. Celino, B. Schönfeld, J.F. Löffler, Icosahedral superclusters in $Cu_{64}Zr_{36}$ metallic glass, Phys. Rev. B 90 (2014), 144108.
[25] J. Ding, Y.Q. Cheng, E. Ma, Full icosahedra dominate local order in $Cu_{64}Zr_{34}$ metallic glass and supercooled liquid, Acta Mater. 69 (2014) 343–354.
[26] R.E. Ryltsev, B.A. Klumov, N.M. Chtchelkatchev, K.Y. Shunyaev, Cooling rate dependence of simulated $Cu_{64.5}Zr_{35.5}$ metallic glass structure, J. Chem. Phys. 145 (2016), 034506.
[27] S. Plimpton, Fast parallel algorithms for short-range molecular dynamics, J. Comput. Phys. 117 (1995) 1–19.
[28] Y.Q. Cheng, E. Ma, H.W. Sheng, Atomic level structure in multicomponent bulk metallic glass, Phys. Rev. Lett. 102 (2009), 245501.
[29] X.X. Yue, C.T. Liu, S.Y. Pan, A. Inoue, P.K. Liaw, C. Fan, Effect of concentration on the structure of isothermally-annealed CuZr metallic glasses, Mater. Sci. Tech-Lond. 34 (2018) 2287–2293.
[30] K.W. Park, H. Park, E. Fleury, Strain localization in annealed $Cu_{50}Zr_{50}$ metallic glass, Mater. Sci. Eng. A 528 (2011) 5319–5326.
[31] W. Mickel, S.C. Kapfer, G.E. Schröder-Turk, K. Mecke, Shortcomings of the bond orientational order parameters for the analysis of disordered particulate matter, J. Chem. Phys. 138 (2013), 044501.
[32] T. Kawasaki, H. Tanaka, Formation of a crystal nucleus from liquid, Proc. Natl. Acad. Sci. 107 (2010) 14036–14041.
[33] Y.D. Wei, P. Peng, Z.Z. Yan, L.T. Kong, Z.A. Tian, K.J. Dong, R.S. Liu, A comparative study on local atomic configurations characterized by cluster-type-index method and Voronoi polyhedron method, Comput. Mater. Sci. 123 (2016) 214–223.
[34] G. Qin, H. Xie, H. Pan, Y. Ren, A new class of ordered structure between crystals and quasicrystals, Acta Metall. Sin. 54 (2018) 1490–1502.
[35] H. Li, C. Fan, K. Tao, H. Choo, P.K. Liaw, Compressive behavior of a Zr-based metallic glass at cryogenic temperatures, Adv. Mater. 18 (2006) 752–754.
[36] J. Zemp, M. Celino, B. Schönfeld, J.F. Löffler, Crystal-like rearrangements of icosahedra in simulated copper-zirconium metallic glasses and their effect on mechanical properties, Phys. Rev. Lett. 115 (2015), 165501.
[37] K. Albe, Y. Ritter, D. Şopu, Enhancing the plasticity of metallic glasses: shear band formation, nanocomposites and nanoglasses investigated by molecular dynamics simulations, Mech. Mater. 67 (2013) 94–103.
[38] X. Xie, Y.C. Lo, Y. Tong, J. Qiao, G. Wang, S. Ogata, H. Qi, K.A. Dahmen, Y. Gao, P.K. Liaw, Origin of serrated flow in bulk metallic glasses, J. Mech Phys. Solids. 124 (2019) 634–642.